Optimal Experimental Design for Parameterization of an Electrochemical Lithium-Ion Battery Model

Saehong Park, [1,z] Dylan Kato,[1] Zach Gima,[1] Reinhardt Klein,[2] and Scott Moura[1]

[1]*Energy, Controls, and Applications Lab, Department of Civil and Environmental Engineering, University of California, Berkeley, California 94720, USA*
[2]*Robert Bosch LLC, Research and Technology Center, Palo Alto, California 94304, USA*

We consider the problem of optimally designing an excitation input for parameter identification of an electrochemical Li-ion battery model. The conventional approach to performing parameter identification uses standard test cycles. In contrast, we optimally design the input trajectory to maximize parameter identifiability in the sense of Fisher information. Specifically, we derive sensitivity equations for the electrochemical model. This approach enables parameter sensitivity analysis and optimal parameter fitting via gradient-based algorithms. This paper presents a general systematic approach to identify the electrochemical parameters in a non-invasive way. First, we group parameters into two sets: (i) equilibrium parameters, and (ii) dynamical parameters. We also divide the dynamical parameters into subsets by calculating orthogonalized sensitivity, which mitigates linear dependence between parameters. A large number of input profiles have been devised to constitute an input library. Then, the optimal inputs are selected from the input library to maximize the Fisher information, via convex programming. Using this framework a number of relevant experiments are obtained to parameterize. To validate our approach experimentally, we consider a 18650 Lithium nickel cobalt aluminum oxide battery. Compared to the conventional approach, our proposal achieves lower voltage RMSE across all experimental testing cycles.
© 2018 The Electrochemical Society. [DOI: 10.1149/2.0421807jes]

Batteries are a key enabling technology behind electrified transportation, portable consumer electronics, and more. To enhance the safety and performance of these devices, one must understand their electrochemical behavior. To this end, battery systems researchers are deeply interested in mathematical electrochemical models. An experimentally validated model can be used for design, simulation and analysis, or online battery management systems (BMS).[1,2] Identifying the unknown model parameters, however, is challenging for multiple reasons. First, battery cell manufacturers do not disclose this information on data sheets for users. Second, one can only measure voltage, current, and temperature - at best. Third, characterizing certain properties, e.g. diffusivities, requires destructive testing. Finally, the measured signals are generally nonlinear with respect to the model parameters, and the dynamics are governed by coupled nonlinear partial differential-algebraic equations.

Accurate electrochemical battery models are critical for a variety of tasks, such as designing high-performance battery management systems, battery pack design, and analysis. However, identifying parameters in electrochemical battery models from measured voltage, current, and temperature data is notoriously difficult. Recently, non-invasive parameter identification of electrochemical models has become an emergent research topic. Schmidt et al.[3] conducted combined parameter analysis and identification by using a Fisher information matrix approach in combination with sensitivity analysis. They use a reduced electrochemical model – a single particle model with electrolyte potential. Recently, Bizeray et al.[4] analyze parameter sensitivity in a single particle model and show it is fully parameterized with six subgroups, under certain mild conditions on the electrode potentials. In contrast, Forman et al.[5] use an "all-in-one" approach to identifying 88 parameters from driving cycle data using a genetic algorithm and the Doyle-Fuller-Newman model. They validate the identified parameter values with experiments and perform Fisher information analysis *ex post facto*. Similarly, authors in Zhang et al.[6] use a multi-objective genetic algorithm called NSGA-II for a LiFePo$_4$ cell. They use terminal voltage and surface temperature as identification objectives. In other work by Zhang et al.,[7] they propose the "Best Practicable Conditions" for each parameter based on sensitivity analysis and clustering analysis. They derived the best identification strategy for each parameter under this condition. The authors also conduct an experimental design which attempts to identify

highly sensitive parameters to poorly sensitive parameters. Recently, both Jobman et al.[8] and Jin et al.[9] propose a two-step procedure that sequences parameter identification. The thermodynamic parameters are identified first, and then the kinetic parameters are identified second via pulses and/or electrochemical impedance spectroscopy (EIS).

Rather than identify all the parameters, some researchers focus on identifying specific subsets of parameters, such as battery health-related or kinetic parameters. For example, the physical parameters, such as diffusion coefficients and activation energies are targeted in [6]. In Marcicki et al.,[10] the authors focus on the electrochemical parameters related to power and capacity fade, as well as their temperature dependence under a variety of charge sustaining and depleting experiments. In Vazquez-Arenas et al.,[11] the researchers analyze sensitivity of certain key parameters using Analysis of Variations (ANOVA), and identify the kinetic and transport parameters with standard test cycles.

Most existing literature on battery parameter identification focuses on parameter fitting, namely, matching model output to experimental data. However, it is unclear if the experimental data is "sufficiently rich" to identify the parameters. A small set of publications in the battery parameter identification literature directly address this problem by formulating an input trajectory optimization problem.[12,13] This work optimizes the amplitude and frequency of a sinusoidal input signal to maximize the Fisher information matrix, for an equivalent circuit model and single particle model, respectively. One could exploit a series of inputs that excite specific parameter sensitivity, however, collecting the required data from experiments can be cost and time intensive. This motivates the following question: Which inputs should be applied to maximize parameter identifiability in a systematic way? In addition, the estimated parameters should be characterized by confidence intervals. These questions motivate optimal experimental design (OED), which provides an important link between experimental design and modeling.[14] In this paper, we propose an electrochemical model-based optimal experiment design framework that yields parameter estimates with statistical information. Instead of formulating a nonlinear trajectory optimization problem, we propose a convex input selection problem.

The paper is organized as follows. First, we briefly presents the DFN electrochemical Li-ion battery model. We generalize this battery model and describe the mathematical background for experimental design. Next section details the proposed optimal experimental design for parameter identification. After that, we present the experimental
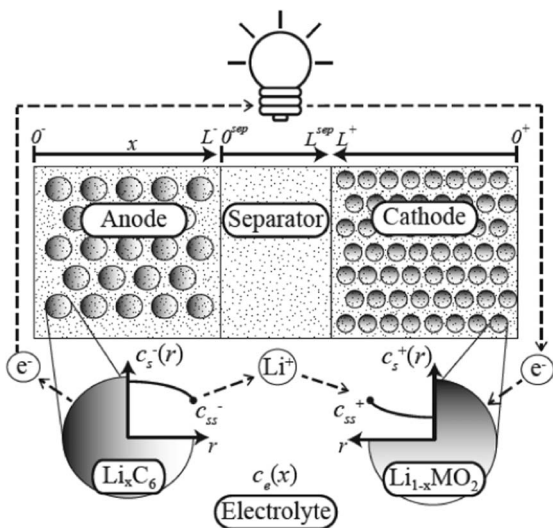
zE-mail: sspark@berkeley.edu

Figure 1. The schematic of first principles electrochemical model known as Doyle-Fuller-Newman (DFN) model.

identification process and a comparison with a conventional approach. In Conclusions section, we summarize our work and provide perspectives on future work.

Electrochemical Battery Model

Doyle-Fuller-Newman (DFN) model.—We consider the Doyle-Fuller-Newman (DFN) model to predict the evolution of lithium concentration in the solid $c_s^\pm(x, r, t)$, lithium concentration in the electrolyte $c_e(x, t)$, solid electric potential $\phi_s^\pm(x, t)$, electrolyte electric potential $\phi_e(x, t)$, ionic current $i_e^\pm(x, t)$, molar ion fluxes $j_n^\pm(x, t)$, battery core temperature $T_1(t)$, and surface temperature $T_2(t)$.[15,16] The schematic of DFN model is shown in Figure 1. The model describes the transport of Li-ions goveneed by diffusion in solid and liquid phase as well as charge conservation in both eletrode. The govening equations are summarized in Appendix A.

Parameter of interest.—The electrochemistry-based battery model combined with two-state thermal dynamics summarized in Appendix B is capable of high-fidelity simulations. However, it has a large number of parameters that must be identified for experimental data. Next, we distinguish fixed parameters from those we seek to identify from data. We classify parameters into two categories: fixed geometric/thermal parameters in Table I and electrochemical parameters listed in Table II.

For the fixed parameter category, we directly measure the geometric parameters and adopt the thermal parameters for a cylindrical 18650 cell from the literature.[6] We then divide the electrochemical parameters in Table II into two groups: equilibrium parameters and dynamical parameters. By "dynamical parameters", we mean parameters associated with the dynamics. There are 21 to-be-identified parameters in total. The equilibrium parameters are closely related to the cell charge capacity. The dynamical parameters characterize the internal dynamics of the battery, e.g. diffusion, ion transport, ohmic overpotential and electrochemical reactions. Due to the wide range of dynamical parameter values, we apply normalization. Parameter θ_i is normalized to $\bar{\theta}_i$ according to:

$$\text{Logarithmic scale}: \quad \bar{\theta}_i = \frac{\log \theta_i - \log \theta_{i,\min}}{\log \theta_{i,\max} - \log \theta_{i,\min}},$$

$$\text{Linear scale}: \quad \bar{\theta}_i = \frac{\theta_i - \theta_{i,\min}}{\theta_{i,\max} - \theta_{i,\min}}, \qquad [1]$$

where each parameter's upper and lower bound is determined from the existing literature values, and possibly any a priori knowledge of the physically meaningful parameter values.

System Generalization

Next, we abstract the electrochemical battery model into a general dynamical system format to formulate our optimal experimental design approach. The dynamical system notation is shown in Table III. In particular, the DFN model is represented by differential algebraic equations (DAEs) after discretizing A1–A21 in space via a suitable method, e.g. finite differences, Padé approximation, spectral methods (see e.g.[17–20]):

$$\dot{\mathbf{x}} = f(\mathbf{x}, \mathbf{z}, u, \theta), \quad \mathbf{x}(t_0) = \mathbf{x_0}, \qquad [2]$$

$$\mathbf{0} = g(\mathbf{x}, \mathbf{z}, u, \theta), \quad \mathbf{z}(t_0) = \mathbf{z_0}, \qquad [3]$$

$$\mathbf{y} = h(\mathbf{x}, \mathbf{z}, u, \theta). \qquad [4]$$

Denote $\mathbf{x} = [c_s^-, c_s^+, c_e, T_1, T_2]^T \in \mathbb{R}^{n_x}$ as the state vector, $\mathbf{z} = [\phi_s^-, \phi_s^+, i_e^-, i_e^+, \phi_e, j_n^-, j_p^+]^T \in \mathbb{R}^{n_z}$ as the algebraic variable vector, $\mathbf{y} = V(t)$ as the output variable defined in A21. Importantly, $\theta = [D_s^-, D_s^+, \ldots, c_e^0] \in \mathbb{R}^{n_p}$ is the vector of dynamical parameters in Table II which we seek to identify.

Sensitivity analysis is used to understand how a model's output depends on variations in the parameter values.[21] Based on nominal parameter values, local sensitivity analysis measures the effects of small changes in the parameters have on the output. For continuous dynamical systems, the local sensitivities are defined as the first-order partial derivatives of the system output with respect to the parameters. We briefly introduce how to derive local sensitivities in dynamical systems described by 2–4. Subsequently, we develop

Table I. Fixed geometric/thermal parameters.

Geometric parameters	
Symbol	Description [SI units]
L^-	Thickness of negative electrode [m]
L^{sep}	Thickness of separator [m]
L^+	Thickness of positive electrode [m]
A	Electrode current collector area [m^2]
Thermal parameters	
Symbol	Description [SI units]
C_1	Heat capacity of battery core [J (m^2 K)$^{-1}$]
C_2	Heat capacity of battery surface [J (m^2 K)$^{-1}$]
h_{12}	Heat transfer coefficients from core to surface [W (m^2 K)$^{-1}$]
h_{2a}	Heat transfer coefficients from surface to ambient [W (m^2 K)$^{-1}$]
$E_{\{D_s^\pm, D_e, \kappa, k^\pm\}}$	Activation energy for Arrhenius temperature dependence [kJ mol^{-1}]

Table II. Parameters of interest for identification.

Equilibrium parameters		
Symbol	Description [SI units]	Normalization scheme
ϵ_s^-	Solid-phase volume fraction [-]	-
ϵ_s^+	Solid-phase volume fraction [-]	-
$n_{\mathrm{Li},s}$	Moles of cyclable lithium in solid phase [mol]	-
Dynamical parameters		
Symbol	Description [SI units]	Normalization scheme
D_s^-	Solid-phase diffusion coefficients of the anode [m^2 s^{-1}]	Logarithmic
D_s^+	Cathode solid-phase diffusion coefficients of the cathode [m^2 s^{-1}]	Logarithmic
R_s^-	Solid-phase particle radii of the anode [m]	Linear
R_s^+	Solid-phase particle radii of the cathode [m]	Linear
σ^-	Solid-phase conductivity of the anode [S m^{-1}]	Logarithmic
σ^+	Solid-phase conductivity of the cathode [S m^{-1}]	Logarithmic
$D_e(\cdot)$	Electrolyte diffusion coefficient [m^2 s^{-1}]	Linear
ϵ_e^-	Electrolyte volume fraction [-]	Linear
$\epsilon_e^{\mathrm{sep}}$	Electrolyte volume fraction [-]	Linear
ϵ_e^+	Electrolyte volume fraction [-]	Linear
$\kappa(\cdot)$	Electrolyte conductivity [S m^{-1}]	Linear
t_c^0	Transference number [-]	Linear
$\frac{d \ln f_{c/a}}{d \ln c_e}(\cdot)$	Activity coefficient [-]	Linear
k^-	Kinetic rate constants [(A m^{-2})(m^3 mol^{-1})$^{(1+\alpha)}$]	Logarithmic
k^+	Kinetic rate constants [(A m^{-2})(m^3 mol^{-1})$^{(1+\alpha)}$]	Logarithmic
R_f^-	Film resistance [Ω m^2]	Linear
R_f^+	Film resistance [Ω m^2]	Linear
$c_e(x, 0)$	Initial Li-ion concentration in electrolyte [mol m^{-3}]	Linear

this approach toward a parameter estimation framework via Fisher information.

Define sensitivity variables as follows:

$$S_\mathbf{x} = \frac{\partial \mathbf{x}}{\partial \bar{\boldsymbol{\theta}}}, \quad S_\mathbf{z} = \frac{\partial \mathbf{z}}{\partial \bar{\boldsymbol{\theta}}}, \quad S_\mathbf{y} = \frac{\partial \mathbf{y}}{\partial \bar{\boldsymbol{\theta}}}, \qquad [5]$$

where $S_\mathbf{x} \in \mathbb{R}^{n_x \times n_p}$, $S_\mathbf{z} \in \mathbb{R}^{n_z \times n_p}$, $S_\mathbf{y} \in \mathbb{R}^{n_y \times n_p}$ are sensitivity matrices. The i, j matrix element is defined as the partial derivative of the i-th variable to the j-th normalized parameter, e.g.

$$[S_\mathbf{x}]_{i,j}(t) = \frac{\partial x_i(t)}{\partial \bar{\theta}_j}. \qquad [6]$$

The evolution of the sensitivity variables is governed by the sensitivity differential algebraic equations (SDAEs), which can be derived following the procedure in [22]:

$$\frac{d}{dt} S_\mathbf{x} = \frac{\partial \boldsymbol{f}}{\partial \mathbf{x}} S_\mathbf{x} + \frac{\partial \boldsymbol{f}}{\partial \mathbf{z}} S_\mathbf{z} + \frac{\partial \boldsymbol{f}}{\partial \boldsymbol{\theta}}, \quad S_\mathbf{x}(0) = S_{\mathbf{x}0}, \qquad [7]$$

$$0 = \frac{\partial \boldsymbol{g}}{\partial \mathbf{x}} S_\mathbf{x} + \frac{\partial \boldsymbol{g}}{\partial \mathbf{z}} S_\mathbf{z} + \frac{\partial \boldsymbol{g}}{\partial \boldsymbol{\theta}}, \quad S_\mathbf{z}(0) = S_{\mathbf{z}0}, \qquad [8]$$

$$S_\mathbf{y} = \frac{\partial \boldsymbol{h}}{\partial \mathbf{x}} S_\mathbf{x} + \frac{\partial \boldsymbol{h}}{\partial \mathbf{z}} S_\mathbf{z} + \frac{\partial \boldsymbol{h}}{\partial \boldsymbol{\theta}}. \qquad [9]$$

The advantage of SDAEs is that they provide a rigorous mathematical computation of the sensitivities compared to a perturbation method where sensitivities are obtained by perturbing each parameter

slightly and calculating the output difference with respect to nominal parameters. Note that SDAEs are linear time-varying DAEs, where the Jacobians are computed at each time step. The Jacobians can be derived analytically by-hand, or calculated numerically via finite differences. In this work, we utilize automatic differentiation since it provides accurate, automated, and fast Jacobian calculations. In particular, we use CasADi,[23] which efficiently computes the first and second-order derivatives. In this work, the battery model DAEs and the corresponding SDAEs are simulated by using the IDAS integrator provided by SUNDIALS via the CasADi interface.[24] Besides convenience for simulation, the automatic calculation of Jacobians provides advantages for optimal experiment design and parameter estimation, as described in the following sections.

Optimal Experimental Design

In this section, we propose a systematic framework for Li-ion battery parameter identification. The following three-step identification process takes account of experimental design blocks in Figure 2.

Step 1: Equilibrium parameter identification

- Run OCV experiment
- Non-linear Least-Squares

Step 2: Sensitivity analysis for dynamical parameters

- Design Input Library
- Sensitivity Analysis
- Grouping Parameters

Step 3: Experimental design for dynamical parameter identification

- Experimental Measurement Error Quantification
- OED-CVX programming
- Design Optimal Input

Table III. DAE notation for the electrochemical model.

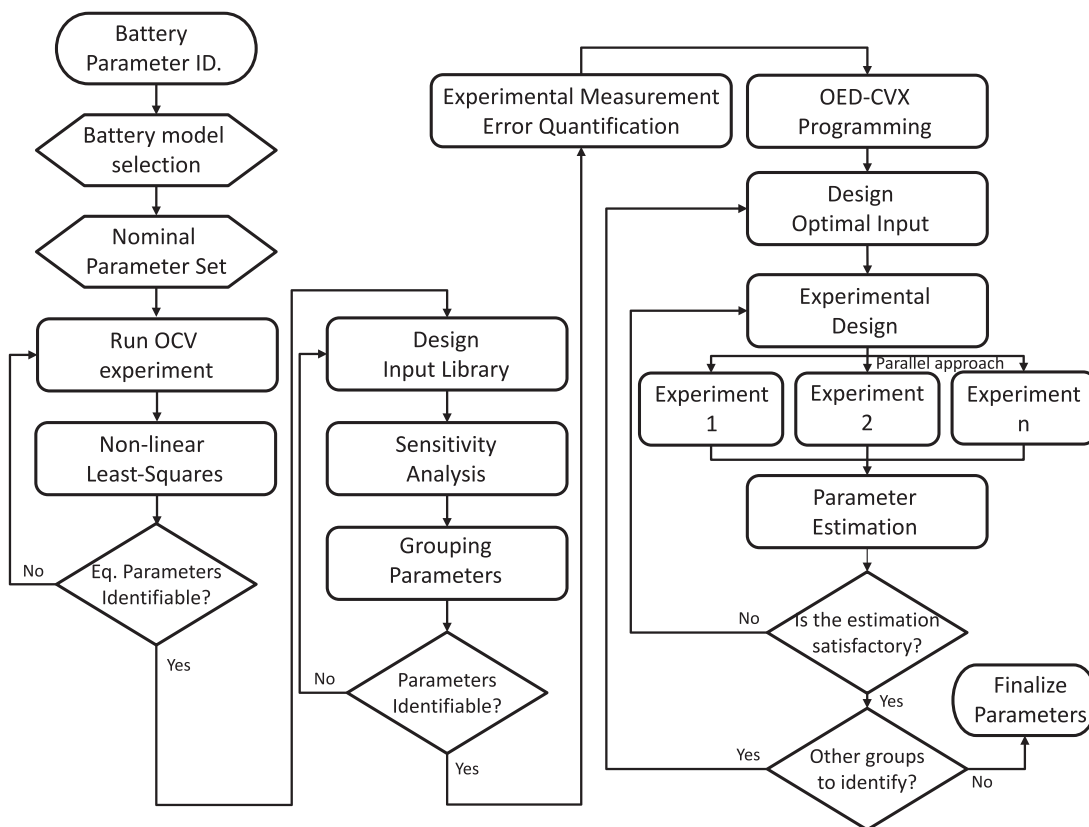| DAE Variables	DFN Variables
$\mathbf{x}$	$c_s^-, c_s^+, c_e, T_1, T_2$
$\mathbf{z}$	$\phi_s^-, \phi_s^+, i_e^-, i_e^+, \phi_e, j_n^-, j_p^+$
u	I
$\boldsymbol{\theta}$	dynamical parameters in Table II

Figure 2. The proposed model-based design of experiments framework for parameter identification of the DFN model.

- Experimental Design
- Parameter Estimation

As a first step, one should select a mathematical model to represent the system under study. The mathematical model considered here is the DFN model. The DFN model mathematically takes the form of DAEs. Once the battery model is selected, then nominal parameter values must be determined. It is important to note that finding nominal parameter values near the true values is beneficial, since the optimal parameter fitting algorithms are based on gradient-descent approach and therefore converge to local minima. We searched relevant papers to choose credible nominal values.

After setting nominal parameter values, we separate the parameters into two groups: equilibrium parameters and dynamical parameters. For equilibrium parameter identification, we adopt the method in [25]. Note that it is possible to derive sensitivity values for equilibrium parameters, however, these values turned out to be dependant on the initial states, resulting in non-zero values for zero currents. For this reason, we solve the non-linear least square problem using data generated from an open circuit voltage (OCV) experiment, which applies very low rate charge/discharge cycles to characterize the equilibrium state. To estimate the dynamical parameters, we generate an input library of possible input trajectories. The sensitivities for each input trajectory are calculated in the library. Then we partition the dynamical parameters into groups, based on their sensitivity magnitudes. High sensitivity parameter groups should be identified first, followed by less sensitive parameters groups.

After grouping the parameters, we run optimal experimental design via convex programming to select optimal inputs for parameter estimation. We use the open-source cvx solver to select optimal inputs. Then, corresponding experiments are executed to collect experimental measurements. For the experimental setup, we utilize a PEC Corp. SBT2050 series tester and Espec environmental chamber.

Once experimental measurements are acquired, the parameter estimation algorithm is applied to fit the simulation result to experimental measurements. In this work, we utilize the Levenberg-Marquardt algorithm for parameter updates at each iteration. We repeat this process until each parameter group is complete. Once we finalize the identified parameters, we compare the identified model output predictions versus a testing data set. For comparison, we benchmark our proposed approach against simple discharge and charge current profiles, which we refer to as a "conventional approach". The following subsections contain detailed analysis for each step of the proposed model-based design of experiments.

Equilibrium parameter identification.—We formulate a procedure to identify parameters in the equilibrium structure of electrochemical models. In words, these parameters correspond to cyclable lithium in the solid phase $n_{Li,s}$ [mol], electrode capacity $Q^{\pm}$ [Ah], and the stoichiometric points $\theta^{\pm}$ [-]. Note, in this subsection we overload the symbol θ to represent stochiometric points to remain consistent with the literature. To identify these parameters, we require experimentally obtained open circuit voltage (OCV) data and known open circuit potential functions for each electrode $U^{\pm}(\cdot)$. Open circuit potentials for each electrode are carefully measured from half cells constructed from the commercial cell. Knowledge of the individual open circuit potentials, $U^{\pm}(\cdot)$ is required for equilibrium parameter identification, a finding that is consistent with existing literature [4,8,9]. We adopt the procedure from a patent by one of the co-authors.[25]

Consider the equilibrium structure of the electrochemical model described in [15]. The relationship between cyclable lithium $n_{Li,s}$ and normalized electrode concentrations $\theta^{\pm}$ is given by:

$$n_{Li,s} = \varepsilon_s^- L^- A \, c_{s,\max}^- \cdot \theta^-(k) + \varepsilon_s^+ L^+ A \, c_{s,\max}^+ \cdot \theta^+(k), \quad \forall \, k,$$
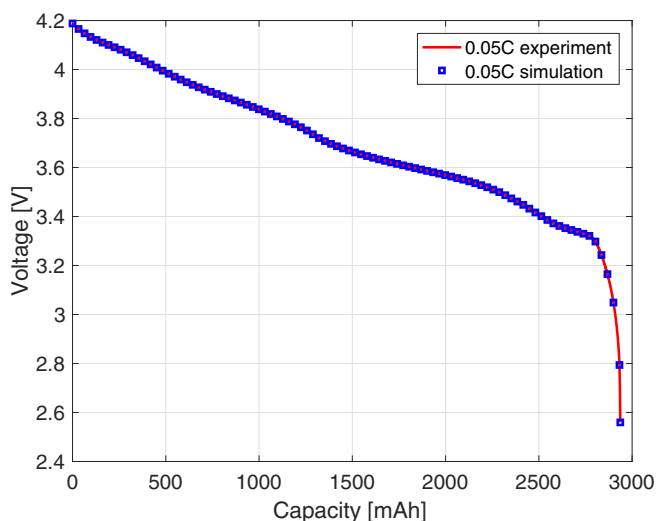
$$[10]$$

Figure 3. OCV comparison between identified model and experimental data for three averaged C/50 charge/discharge cycles.

where k indexes stochiometric points parameterized by time or Ah-processed. For convenience, let us define the lumped parameters $H^{\pm}$ as

$$H^{\pm} = \varepsilon_s^{\pm} L^{\pm} A \cdot c_{s,\max}^{\pm}. \qquad [11]$$

Dimensional analysis reveals that $H^{\pm}$ have dimensions of [mol]. Consequently, we define $H^{\pm}$ to be the molar capacity of the electrodes. The charge capacity of the electrodes is therefore given by:

$$Q^{\pm} = F \cdot H^{\pm}, \qquad [12]$$

where F is Faraday's constant. Then, let us define a recursive relationship that relates the steady-state normalized anode concentrations before and after injecting current I for Δt time units.

$$\theta^{-}(k+1) = \theta^{-}(k) - \frac{\Delta t}{F H^{-}} \cdot I, \qquad \forall k. \qquad [13]$$

The equilibrium voltage, i.e. OCV, is given by:

$$V(k) = U^{+}(\theta^{+}(k)) - U^{-}(\theta^{-}(k)), \qquad \forall k. \qquad [14]$$

Solving 10 for $\theta^{+}(k)$ and substituting into 14 gives:

$$V(k) = U^{+}\left(\frac{n_{Li,s} - H^{-}\theta^{-}(k)}{H^{+}}\right) - U^{-}(\theta^{-}(k)), \qquad \forall k. \qquad [15]$$

To summarize, we have unknowns $x = \left[\theta^{-}(0), H^{+}, H^{-}, n_{Li,s}\right]^{T}$ and Equations 13, 15. Then, we formulate the following nonlinear optimization problem to find the unknown variables x given experimentally obtained cell OCV data $V_{ocv}(k)$ and known open circuit potential functions $U^{\pm}(\theta^{\pm})$:

$$\underset{x}{\text{minimize}} \sum_{k=0}^{N} \left[V(k) - V_{ocv}(k)\right]^{2}, \qquad [16]$$

$$\text{subject to}: \quad V(k) = U^{+}\left(\frac{n_{Li,s} - H^{-}\theta^{-}(k)}{H^{+}}\right) - U^{-}(\theta^{-}(k)), \quad \forall k, \qquad [17]$$

$$V^{\max} = U^{+}\left(\frac{n_{Li,s} - H^{-}\theta^{-}(0)}{H^{+}}\right) - U^{-}(\theta^{-}(0)), \qquad [18]$$

$$\theta^{-}(k+1) = \theta^{-}(k) - \frac{\Delta t}{F H^{-}} \cdot I, \qquad \forall k = 0, 1, \cdots, N-1, \qquad [19]$$

where N is the total number of experimental data points, and $V^{\max}$ corresponds to the maximum OCV and the first index $k = 0$. Note the last constraint is initialized with optimization variable $\theta^{-}(0)$. This

Table IV. Identified equilibrium parameters.

Parameter	Estimated values
ε_s^{-}	5.438895e-01
ε_s^{+}	6.663649e-01
$n_{Li,s}$	0.1406 moles

optimization program is nonlinear and non convex in the optimization variables, requiring a nonlinear optimization solver, such as `fmincon` in Matlab.

Suppose that $\theta^{\pm}(0)^{\star}$ and $\theta^{\pm}(N)^{\star}$ correspond to the optimized normalized concentrations at the maximum and minimum voltage limits, respectively, according to the cell's datasheet. Then the stochiometric points are given by:

$$\underline{\theta}^{\pm,\star} = \theta^{\pm}(0)^{\star}, \qquad \overline{\theta}^{\pm,\star} = \theta^{\pm}(N)^{\star}. \qquad [20]$$

Suppose that $H^{\pm,\star}$ correspond to the optimized molar capacities of each electrode. Then the charge capacity of each electrode $Q^{\pm,\star}$ and the cell $Q^{\star}$ can be calculated as:

$$Q^{\pm,\star} = F \cdot N^{\pm,\star}, \qquad Q^{\star} = \min\left\{Q^{+,\star}, Q^{-,\star}, F \cdot n_{Li,s}^{\star}\right\}. \qquad [21]$$

By solving the optimization problem 16–19 using OCV data from three averaged C/50 charge/discharge cycles, we obtain the following equilibrium parameters as shown in Table IV.

Figure 3 compares the identified equilibrium model against experimental data. We achieve an overall root mean square error (RMSE) of less than 5 mV in 98% of the operating range. If one uses faster OCV tests, e.g. C/25, C/10, or C/5, then the resulting model identification accuracy will degrade. Based on the identified structure, we define the cell state-of-charge (SOC) in association with the equilibrium voltage as listed in Table V, which is used for simulation and experiment design in subsequent sections.

Sensitivity analysis for dynamical parameters.—Next we identify the dynamic parameters in Table II. A fundamental challenge is linear dependence between the parameter sensitivities, resulting in non-uniqueness between estimated parameter values. For this reason, we adopt a parameter grouping-based approach.[3] In our approach, each parameter's sensitivity is analyzed across a large number of input profiles.

In order to design the optimal set of experiments for identifying battery parameters, a suite of candidate input profiles has been generated. The input library is heuristically designed to cover a wide range of frequency content and current magnitudes. Broadly, these candidate profiles can be categorized as 1) pulses, 2) sinusoids, and 3) driving cycles. The profiles were generated by a custom Matlab script, which iterated across several design parameters for each input profile category. For example, pulses were generated by various combinations of pulse width, duty ratio, total time, charge/discharge, and initial voltage. Sinusoidal profiles were generated for various combinations of frequency, total profile time, initial voltage, and charge/discharge. The range of input profile characteristics, e.g. frequency, was determined with consideration for hardware limitations of our battery tester, computational limits/time, and aliasing phenomenon. In all cases, the input magnitudes were normalized such that their L1 norm is 1 Ah, thereby enabling a fair comparison between inputs. A total of 738 profiles exists across these three input categories. Setting constraints that de-

Table V. Cell SOC to voltage mapping.

SOC	Voltage mapping [V]
80%	3.9481
60%	3.7689
40%	3.5982
20%	3.4562

Table VI. Pulse profile specification.

Input variable	Setting
Amplitude	0.5C to 5C, in 0.5C increments
Pulse width	1 sec to 1000 sec
Duty cycle	$n * $ (pulse width), $n \in \{1, 2, 3\}$
Total time	600 sec (10 min) to 3600 sec (1 hr)
Initial voltage	$V_0 = \{3.9481\ 3.7689\ 3.5982\ 3.4562\}$
Current	charge only, discharge only, or both

fine the feasible set of input profiles is the first step in evaluating the candidate input profiles. Across all profile categories, the following constraints must be upheld:

1. $T_2 \leq 50^o C$
2. $|I(t)| \leq 5C$
3. $600\ \text{sec} \leq t_f \leq 3600\ \text{sec}$

Additionally, all input profiles are generated from the following initial SOC: $SOC_0 \in \{0.8, 0.6, 0.4, 0.2\}$. The initial voltage V_0 values associated with initial SOC are determined according to the Table V. On the other hand, input profiles need to keep the SOC within its upper and lower limit. To check that these conditions hold, the absolute ΔSOC for each profile is calculated and added to SOC_0. The immediate conclusions are that driving cycle profiles, all of which are net discharging, cannot be applied when the battery SOC is 20%. Similarly, discharging pulse and sinusoid profiles cannot be applied when the battery SOC is 20%. Charging pulse and sinusoid profiles cannot be applied for SOC $\geq$ 80%. Consequently, these inputs are parsed out of the input library. The remainder of this section will describe the parameters of each profile category and its corresponding normalization scheme.

Pulse profiles are generated with six input variables for a total of 540 pulse profiles as shown in Table VI. Note that the pulse width upper bound is set to be commensurate with the characteristic diffusion time for a given battery chemistry. The current values are normalized using an L_1 norm, i.e. the integral of the current magnitude over the total time of the profile: $I(t)/\int |I(t)|dt$. Therefore, the total normalized amount of charge processed in each pulse is equal to 1 Ah.

Sinusoid profiles are generated with four input variables for a total of 180 sinusoid profiles, as detailed in Table VII. Note that the frequency range was set in order to: (i) avoid exciting dynamics occurring at un-modeled frequencies, and (ii) not violate the sampling rate limit of a standard battery tester. The current values are also normalized with the L_1 norm, i.e. the integral of the current magnitude over the total time of the profile: $I(t)/\int |I(t)|dt$. Therefore, the total normalized amount of charge processed in each pulse is equal to 1 Ah. Charge only, discharge only, and charge-discharge profiles follow the same structure as the pulse profiles.

The dynamic drive cycle profiles summarized in Table VIII are evaluated at three different initial SOCs, for a total of 18 dynamic drive cycle profiles. Note that US06 is the most aggressive cycle in terms of peak current applied. The current values are normalized to the L_1 norm so that the total normalized amount of charge processed in each pulse is equal to 1 Ah.

There are 540 pulse inputs, 180 sinusoidal inputs, and 18 driving cycle inputs, yielding a total of 738 inputs and 329.65 hours in

Table VIII. Driving cycle profile specification.

Name	Description
DC1	naturalistic morning driving test profile[26]
DC2	nautralistic evening driving test profile[26]
LA92	Unified driving schedule for emission inventory[27]
SC04	Speed correction driving schedule[27]
UDDS	Urban dynamometer driving schedule[27]
US06	High acceleration aggressive driving schedule[27]

the input library. Note that short duration input profiles tend to have large input magnitudes due to normalization while long duration input profiles have relatively small input magnitudes. High performance computing cluster is used to parallelize model simulation and sensitivity calculations.

When input library in constructed, we introduce the parameter grouping methodology for parameter identification. It is well known (see e.g.[5]) that the entire electrochemical parameter vector θ is weakly identifiable from the measured output, since the system is nonlinear in the parameters. This is due to linear dependence between the parameter sensitivity vectors.[3] When the linear dependence exists in parameter sensitivity vector space, an output produces nearly identical reactions when two different parameters are perturbed. Therefore, it is necessary to analyze the linear dependence between electrochemical parameters, and rank/organize them into groups to avoid non-unique solutions during the parameter identification process. Suitable linear transformations of $S_\mathbf{y}^T S_\mathbf{y}$ can reveal properties such as norm and linear dependence.[28] Orthogonalization allows us to systematically rank the most influential parameters on the model output.

For parameter grouping, we first perform sensitivity analysis across the library of input profiles. After calculating the sensitivities [7–9] for 738 profiles through parallel computing, we apply the Gram-Schmidt process on $S_\mathbf{y}^T S_\mathbf{y}$ to reveal the orthogonalized sensitivity magnitudes and linear dependence.[29] Figure 4 visualizes the average

Table VII. Sinusoid profile specification.

Input variable	Setting
Frequency	$\{0.01, 0.05, 0.1\}$ Hz
Total time	600 sec (10 min) to 3600 sec (1 hr)
Initial voltage	$V_0 = \{3.9481\ 3.7689\ 3.5982\ 3.4562\}$
Current	charge only, discharge only, or both

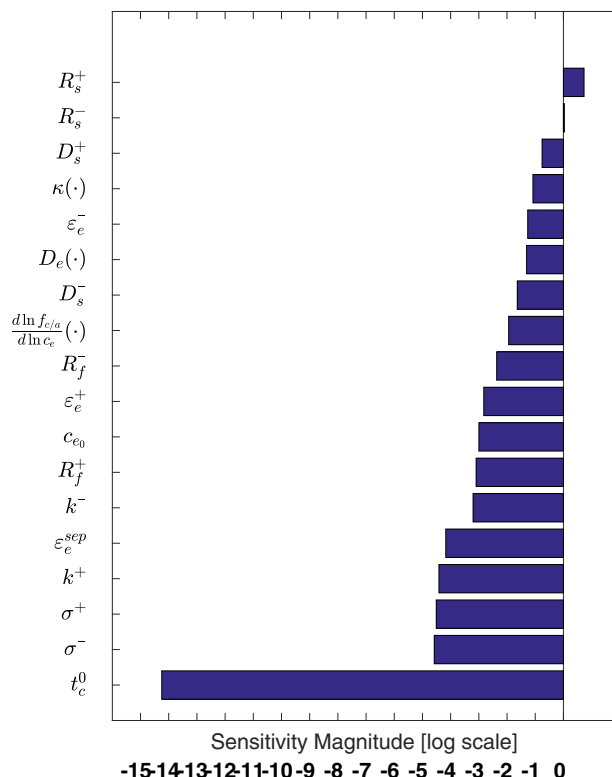**Figure 4.** The sorted average orthogonalized sensitivity magnitudes across all inputs in the input library.

Table IX. Dynamic parameter groups.

Group 1	Group 2	Group 3	Group 4
R_s^-	D_s^-	R_f^-	σ^-
R_s^+	D_s^+	k^-	σ^+
	ε_e^-	ε_e^+	ε_e^{sep}
	$\kappa(\cdot)$	c_{e_0}	k^+
	$D_e(\cdot)$	R_f^+	t_c^0
	$\frac{d\ln f_{c/a}}{d\ln c_e}(\cdot)$		

sensitivity magnitudes via Graham-Schmidt orthogonalization over 738 profiles.

Based on this sensitivity analysis, we group the parameters based on their orthogonalized sensitivity magnitudes. The resultant groups are shown in Table IX. It is evident that some of the parameters have strong identifiability, i.e. particle radii $R_s^\pm$. Other parameters, e.g. the transference number t_c^0 and solid phase conductivities $\sigma^\pm$, are weakly identifiable. To validate these conclusions, we apply a parameter perturbation approach to a parameter from each of the four groups. Figure 5a visually demonstrates that Group 1 parameter R_s^- has the largest impact on voltage, followed by representative parameters in Group 2 (D_s^-), Group 3 (R_f^-), and Group 4 (σ^-). For

fair comparison, we perturb each representative parameter according to its normalized value, denoted by upper bars in Figure 5. Note, one should not expect these conclusions to be generally true across all cell chemistries, models, and manufacturers. These conclusions are specific to the cell under study and normalization.

In the parameter identification framework, Group 1 is identified first, while the other parameters are fixed to their nominal values. Next, Group 2 parameters are identified while fixing the remaining unidentified parameters, and so forth.

Experimental design for dynamical parameter identification.— In statistical experiment design, the amount of "information" on parameter vector $\boldsymbol{\theta}$ contained in the observation $\mathbf{y}$ from an experiment is calculated by the Fisher information matrix, $\mathbf{F}$.[30] The Fisher information matrix is mathematically defined as:

$$\mathbf{F} = \int_0^{t_f} S_\mathbf{y}^T(t) Q(t)^{-1} S_\mathbf{y}(t)\, dt, \qquad [22]$$

where $t \in [0, t_f]$, and $Q(t)$ is the covariance matrix of the measurement error. Since the true parameters $\boldsymbol{\theta}^*$ are unknown, the sensitivity is calculated around nominal parameter values $\boldsymbol{\theta}_0$. The deviation of the parameter estimates from their true values can be expressed as the covariance matrix Σ. According to the Cramer-Rao bound,[31,32] the inverse of the Fisher information matrix provides a lower bound
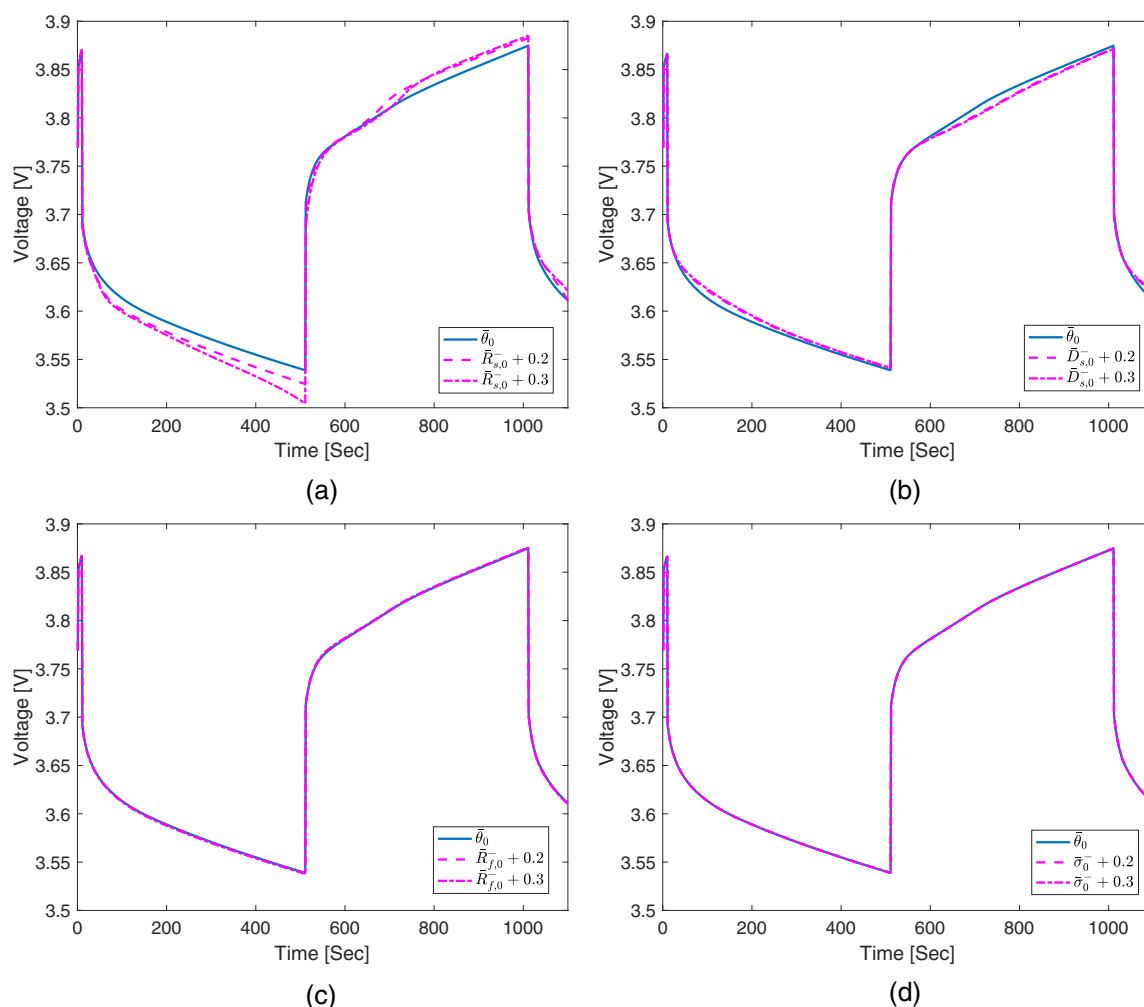

Figure 5. The comparison of model output impact by changing parameters. (a) Perturbation of Group 1 parameter $\overline{R}_s^-$. (b) Perturbation of Group 2 parameter $\overline{D}_s^-$. (c) Perturbation of Group 3 parameter $\overline{R}_f^-$. (d) Perturbation of Group 4 parameter $\overline{\sigma}^-$.

on Σ,

$$\mathbf{F}^{-1} \leq \Sigma. \qquad [23]$$

Our goal is to find inputs that minimize the lower bound of the parameter estimation error, thus improving the parameter estimation quality. To optimize the amount of information, a proper scalarization of $\mathbf{F}$ should be considered. Several scalarization criteria are commonly used in the literature such as:

- D-optimality: $\log \det(\mathbf{F}^{-1})$.
- A-optimality: $\text{trace}(\mathbf{F}^{-1})$.
- E-optimality: $\lambda_{\max}(\mathbf{F})$.

Each optimality criterion has a different geometrical interpretation. For instance, D-optimal design minimizes the geometric mean of the errors in the parameters, while E-optimal design minimizes the largest eigenvalue of the confidence region of parameters. In this work, we use D-optimal design as it is the most commonly used.[14] However, the other criteria are equally applicable in this framework.

We formulate a procedure to optimize experiment design to produce inputs that are maximally informative for parameter estimation. A natural and mathematically elegant approach is to formulate an optimal control problem. Namely, one may seek an input trajectory that maximizes D-optimality subject to the system dynamics. This concept has been applied in [12,13]. However, solving a large-scale optimal control problem with thousands of states and nonlinear dynamics given by 2–4, 7–9 is computationally intractable. Two weeks of wall clock time are needed to optimize a 100 second input trajectory for the electrochemical model on a PC with an INTEL Core i5 - 1.8GHz dual core, Turbo Boost up to 2.9GHz, with 3MB shared L3 cache, and 8GB RAM. The previous literature[12,13] side-steps this challenge using control vector parameterization and simplified models, such as an equivalent circuit model or single particle model.

To bypass the challenge of solving a large-scale nonlinear optimal control problem, we pursue a different approach. Specifically, we seek the set of inputs from an input library which maximizes the Fisher information matrix. This process yields a convex optimization program, which can be rapidly solved with polynomial complexity open-source solvers, such as cvx.[33]

We now detail the theory behind optimal experiment design via convex optimization. Suppose we have a set of L experimental inputs $u_i(t)$, $i = 1, 2, \cdots, L$. For each input profile $u_i(t)$, we obtain a corresponding sensitivity vector $S_{\mathbf{y},i}(t)$ by solving 2–4 and 7–9 simultaneously. Amongst these L inputs $u_i(t)$, $i = 1, 2, \ldots, l$, we select M inputs that are maximally informative as measured by the Fisher information matrix F, where $M < L$. Let $m_j \in \{0, 1\}$ be a binary value that indicates if experiment j is executed from the input library. Then, the total number of experiments is given by

$$m_1 + m_2 + \ldots + m_l = M. \qquad [24]$$

We then rewrite the Fisher information matrix as:

$$\mathbf{F} = \sum_{i=1}^{L} m_i S_{\mathbf{y},i}^T Q_i^{-1} S_{\mathbf{y},i}. \qquad [25]$$

We now formulate a combinatorial optimization problem to maximize the D-optimality criterion of F:

$$\underset{m_i}{\text{minimize}} \quad \log \det \left(\sum_{i=1}^{L} m_i S_{\mathbf{y},i}^T Q_i^{-1} S_{\mathbf{y},i} \right)^{-1}, \qquad [26]$$

$$\text{subject to} \quad m_i \in \{0, 1\}, \qquad [27]$$

$$m_1 + \ldots + m_l = M. \qquad [28]$$

This problem is a binary integer program, where the optimal number of experiments m_i is the solution. In general, large-scale combinatorial problems are NP-hard. In this work, we relax the integer

constraint 27 into $0 \leq m_i \leq 1$, yielding a relaxed optimization problem that is convex. Let $\eta_i = m_i/M$ be the fraction of experiment type i to execute. Then the Fisher information 25 can be re-written as

$$\mathbf{F} = M \sum_{i=1}^{L} \eta_i S_{\mathbf{y},i}^T Q_i^{-1} S_{\mathbf{y},i}, \qquad [29]$$

where $\eta \in \mathbb{R}^L$, $\mathbb{1}^T \eta = 1$. Thus, our final convex optimal experiment design problem is:

$$\underset{\eta}{\text{minimize}} \quad \log \det \left(\sum_{i=1}^{L} \eta_i S_{\mathbf{y},i}^T Q_i^{-1} S_{\mathbf{y},i} \right)^{-1}, \qquad [30]$$

$$\text{subject to} \quad 0 \leq \eta_i \leq \frac{1}{M}, \, \forall i \quad \mathbb{1}^T \eta = 1, \qquad [31]$$

where M can be dropped without affecting the minimizer. One can show this is a convex problem with respect to η.[34] Additionally, the solutions will be integral; that is, the solution to relaxed optimization problem 30–31 is also the solution to 26–27.

Remark: Suppose that associated with each experiment $u_i(t)$ is a cost c_i, which can represent time required, economic/labor cost, or battery degradation. The total cost is:

$$c_1 m_1 + \cdots + c_l m_l = mc^T \eta. \qquad [32]$$

Suppose we have a cost budget of B. One can then add a budget constraint as a scalar linear inequality, yielding convex program:

$$\underset{\eta}{\text{minimize}} \quad \log \det \left(\sum_{i=1}^{L} \eta_i S_{\mathbf{y},i}^T Q_i^{-1} S_{\mathbf{y},i} \right)^{-1}, \qquad [33]$$

$$\text{subject to} \quad 0 \preceq \eta \preceq \frac{1}{M}, \quad \mathbb{1}^T \eta = 1, \qquad [34]$$

$$mc^T \eta \leq B. \qquad [35]$$

Consider the output measurement covariance Q_i in 30. This quantity is critically important to include in the optimization formulation. To motivate this point, consider Figures 6a and 6b which visualize the battery tester's measured voltage for ten repeated pulse inputs. Figure 6a contains time steps in which the measured voltage has variance larger than 30 mV. This variance is uncorrelated with the order in which the experiments are performed. In contrast, the sinusoidal tests in Figure 6b have variance consistently around 0.3 mV. Consequently, there can be non-trivial variation in the battery tester's measured voltage, depending on the input profile. Note, our SBT2050 test system manual claims a voltage resolution of 100 µV. The precise source of the measurement variance is unknown.

This motivates quantification of the output measurement covariance. Namely, 30–31 requires Q_i for each input in the library. However, experimentally characterizing Q_i for each input requires running every experiment in the input library multiple times (e.g. 10 times) – an intractable task. Therefore, we propose to predict the covariance Q_i using a regression model trained from a small number of experiments. This enables us to account for variance in experimental trials without running a large number of experiments.

The size of matrix Q is based on the number of samples taken during an experiment. Due to this, we scalarize Q in order to compare how Q varies across experiments that have different lengths. For a given experiment and its corresponding covariance matrix $Q^{\exp}$, we scalarize $Q^{\exp}$ using the square root of the mean across the diagonal entries of $Q^{\exp}$:

$$q = \sqrt{\frac{1}{n} \sum_{i}^{n} Q_{i,i}^{\exp}}, \qquad [36]$$

where n is the dimension of the matrix Q. Next, we seek a regression model to predict q from the current input profile. To this end, we
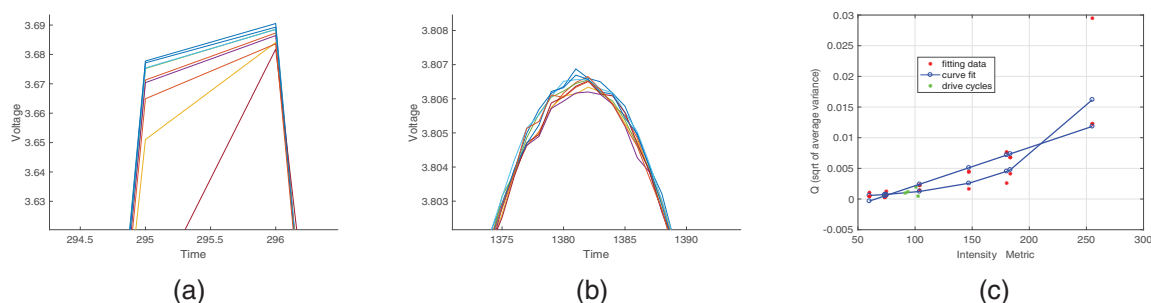
Figure 6. Experimental outputs and quantification. (a) Zoom of multiple, superimposed pulse experimental trials. This experiment has up to 30 mV of measured voltage variance. (b) Zoom of multiple, superimposed sinusoidal experimental trials. This experiment has 0.3 mV of measured voltage variance. (c) Scalarized variance from training data, testing data, and regression model (curve fit).

consider a metric of "input intensity" as the feature in our regression model. Namely, we propose to use the L_2 norm, $\tilde{I}$, to characterize input intensity where

$$\tilde{I} = \sqrt{\int_0^{t_f} I(t)^2 dt}. \qquad [37]$$

Using $\tilde{I}$ as a regression model feature, we fit the following regression models to q:

$$\text{for charge inputs}: \quad \hat{q}_c = a_c \tilde{I} + b_c,$$

$$\text{for discharge inputs}: \quad \hat{q}_d = a_d \cdot e^{b_d \cdot \tilde{I}}, \qquad [38]$$

where $a_c = 6.2382 \times 10^{-5}$, $b_c = -4.0739 \times 10^{-3}$, $a_d = 2.1045 \times 10^{-4}$, $b_d = 1.7020 \times 10^{-2}$. For inputs that are not purely charge or discharge, the two models are averaged:

$$\hat{q}_{cd} = \frac{1}{2}\left(q_c + q_d\right). \qquad [39]$$

The scalar predictions $\hat{q}$ are then squared and constructed into a matrix according to:

$$\hat{Q} = \hat{q}^2 \cdot \mathbb{I}_n, \qquad [40]$$

where $\mathbb{I}_n$ is an $n \times n$ identity matrix. For training, 5 drive cycle profiles are used to estimate the parameters a_c, b_c, a_d, b_d in 38. We test the predicted variance on drive cycle inputs. Data for training and testing is provided in Figure 6c, along with the curve fit regression model predictions.

After obtaining experimental data, we now seek to optimally fit the parameter vector $\boldsymbol{\theta}$ to this data. The optimization problem for parameter identification can be formulated as a nonlinear least squares problem:

$$\underset{\hat{\boldsymbol{\theta}}}{\text{minimize}} \quad \sum_{i=1}^{M} \sum_{k=0}^{k_f} \left[\frac{\mathbf{y}_i(k) - \hat{\mathbf{y}}_i(k; \hat{\boldsymbol{\theta}})}{Q_i(k)} \right]^2, \qquad [41]$$

where k indexes the timed samples, M is the number of optimized input profiles obtained from optimal input design, $\mathbf{y}_i(k)$ is the experimentally measured voltage, $\hat{\mathbf{y}}_i(k; \hat{\boldsymbol{\theta}})$ is the model's voltage prediction, and $Q_i(k)$ is the measurement variance for input profile i at time step k. The Levenberg-Marquardt algorithm is used to update the parameters $\hat{\boldsymbol{\theta}}$ iteratively to solve the nonlinear optimization problem 41. This algorithm adaptively updates the parameter estimates via a hybridization of the gradient descent update and the Gauss-Newton update:[35]

$$\left[\mathbf{J}^T\mathbf{W}\mathbf{J} + \gamma \cdot \text{diag}(\mathbf{J}^T\mathbf{W}\mathbf{J})\right]\Delta\boldsymbol{\theta} = \mathbf{J}^T\mathbf{W}(\mathbf{y} - \hat{\mathbf{y}}), \qquad [42]$$

where $\mathbf{J} = \partial\hat{\mathbf{y}}/\partial\hat{\boldsymbol{\theta}}$ is the local sensitivity of the output $\hat{\mathbf{y}}$, and $\mathbf{W}$ is the inverse of the measurement error covariance matrix, $\mathbf{W} = Q^{-1}$. The value of γ weighs gradient descent update against Gauss-Newton update. Conveniently, the Levenberg-Marquardt algorithm

Table X. Input profiles from optimal experimental design.

Group 1	Group 2	Group 3	Group 4
#339	#90	#292	#120
#342	#120	#365	#343
#345	#339	#467	#362
#348	#345	#503	#503
#365	#365	#507	#507

directly utilizes the Jacobians computed via automatic differentiation, obtained from the sensitivity analysis. Then, the parameter updates are iteratively updated according to:

$$\boldsymbol{\theta}(n+1) = \boldsymbol{\theta}(n) + \Delta\boldsymbol{\theta}, \qquad [43]$$

where n is the iteration index.

After optimally fitting the parameters, estimation error statistics are calculated according to

$$\rho_{\boldsymbol{\theta}} = \mathbf{J}^T\mathbf{W}\mathbf{J}, \qquad [44]$$

$$\sigma_{\boldsymbol{\theta}} = \sqrt{\text{diag}[\mathbf{J}^T\mathbf{W}\mathbf{J}]^{-1}}, \qquad [45]$$

where $\rho_{\boldsymbol{\theta}}$ is the parameter covariance matrix, and $\sigma_{\boldsymbol{\theta}}$ is the standard parameter error. Lastly, 95% confidence intervals for the parameter estimates are calculated as follows:

$$\hat{\boldsymbol{\theta}} - \boldsymbol{t}_{(1-0.05,N)}\frac{\sigma_{\boldsymbol{\theta}}}{\sqrt{N}} \le \boldsymbol{\theta}^* \le \hat{\boldsymbol{\theta}} + \boldsymbol{t}_{(1-0.05,N)}\frac{\sigma_{\boldsymbol{\theta}}}{\sqrt{N}}, \qquad [46]$$

where N is the number of observations, and $\boldsymbol{t}$ is the upper critical value for the t-distribution with $n - 1$ freedom.[36]

Experimental Results

In this section the proposed optimal experimental design is applied to a 18650 Lithium nickel-cobalt-aluminum oxide (NCA) battery cell manufactured by Panasonic, with rated capacity of 2700mAh, Vmax: 4.2V, Vmin: 2.5V, and nominal voltage: 3.6V. To assess the benefits of our proposed approach, we compare results against parameter identification using a conventional approach with standard test cycles.

Parameter identification results.—With consideration for output measurement error covariance Q, the results for optimal input selections for parameter identification are listed in the Table X. The optimized inputs have moderate magnitude and do not increase cell temperature more than 5°C. Based on the sensitivity analysis and parameter grouping, we estimate parameters for each group in a cumulative fashion. For example, we allow the Group 1 parameters to be refined with Group 2 parameters while fitting the model parameter to Group 2 experimental data. Similarly, Group 1 & 2 parameters are refined with Group 3 parameters and so on. Since we do not have
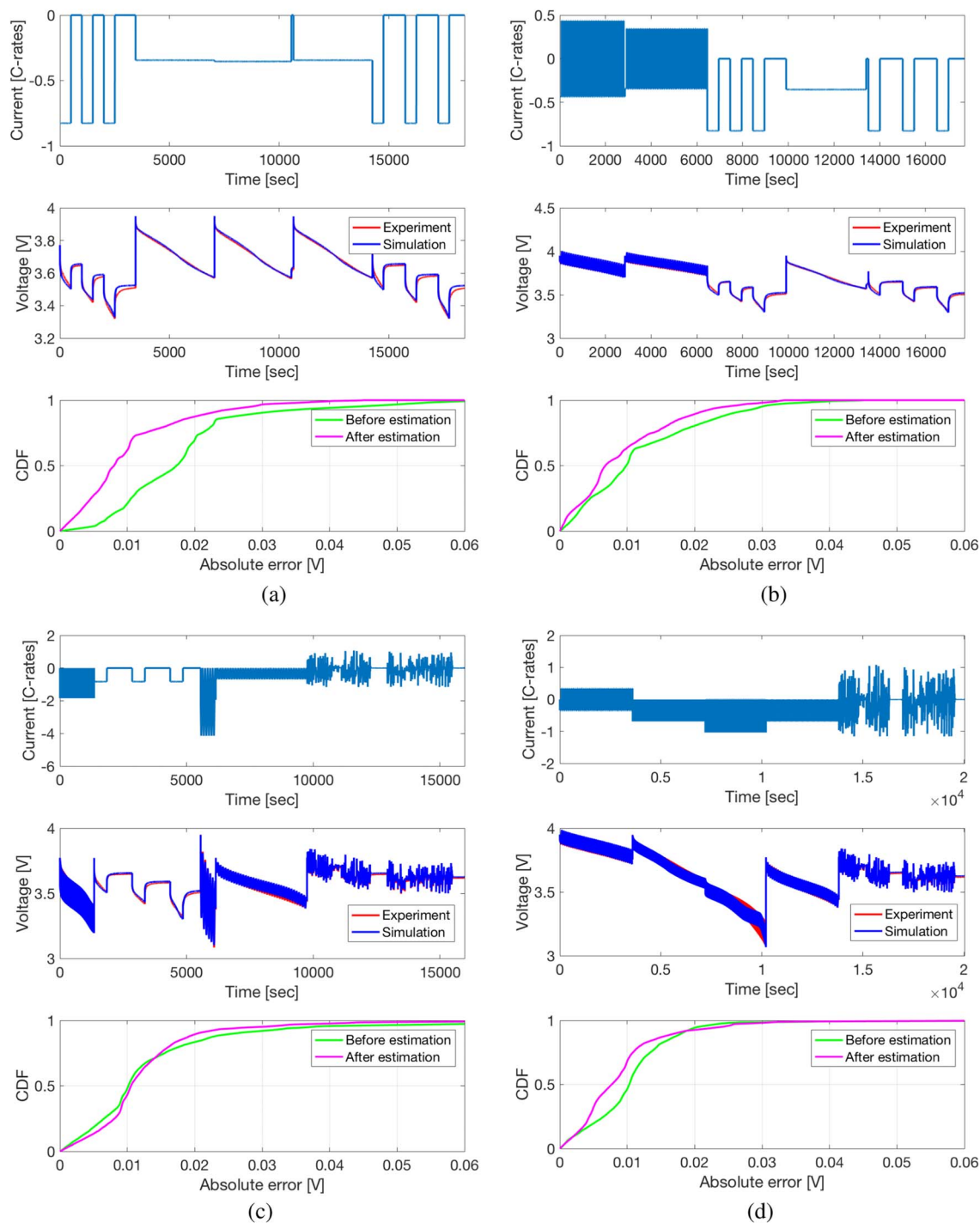
Figure 7. Identification results for optimal designed inputs. (a) Identification results for Group 1 parameters. (b) Identification results for Group 2 parameters. (c) Identification results for Group 3 parameters. (d) Identification results for Group 4 parameters.

information on the true parameters, it is useful to identify the parameters in a cumulative way to prevent overfitting and increase the degrees of freedom during optimization. The authors' previous work also showed that an optimized input reduces the condition number of the objective function's Hessian with respect to the parameters.[37] This accelerates gradient descent methods for parameter estimation.

Figure 7 displays the parameter identification results for each group. For instance, Group 1's optimal input consists of a series of concatenated input profiles with id #339, 342, 345, 348, 365, as shown in Figure 7a. We also plot the identified model's voltage prediction versus the experimentally measured voltage. Finally, the cumulative

distribution function of the absolute voltage prediction error before and after applying parameter estimation are displayed in the bottom subplot. Note the most significant improvements relative to the nominal parameter values come after applying the Group 1 optimized inputs. This is intuitive, as the Group 1 parameters have the greatest sensitivity, by definition.

The final parameter estimates along with their 95% confidence intervals are listed in Table XI. The identified parameter values are also visualized in Figure 8 on a normalized axis, along with the nominal values for comparison. The 95% confidence intervals are also visualized by error bars for each parameter, and correspond to the

Table XI. Final identification results for NCA 18650 Li-ion battery.

Parameter	Unit	Lower	Upper	Nominal	Result	95% C.I.[†]
D_s^-	[m² s⁻¹]	2.25e-16	1.05e-12	3.90e-14	2.634e-14	2.407e-18
D_s^+	[m² s⁻¹]	2.00e-16	1.00e-12	1.00e-13	6.625e-14	1.548e-17
R_s^-	[m]	1.00e-06	1.00e-04	10.9e-06	20.235e-06	8.362e-10
R_s^+	[m]	1.00e-06	1.00e-04	10.9e-06	17.163e-06	7.494e-10
ϵ_s^-	[-]	-	-	-	0.5438	-
ϵ_s^+	[-]	-	-	-	0.6663	-
σ^-	[S m⁻¹]	50	500	100	500	1.740e+03
σ^+	[S m⁻¹]	50	500	100	500	1.334e+02
$D_e(\cdot)$	[m² s⁻¹]	0.5	1.5	1	1.195	1.176e-03
ϵ_e^-	[-]	0.18	0.45	0.3	0.289	3.687e-04
ϵ_e^{sep}	[-]	0.45	0.5	0.5	0.468	5.801e-04
ϵ_e^+	[-]	0.18	0.33	0.3	0.307	5.523e-04
$\kappa(\cdot)$	[S m⁻¹]	0.5	1.5	1	1.398	1.308e-03
t_c^0	[-]	0.36	0.363	0.363	0.36	5.585e-04
$\frac{d\ln f_{c/a}}{d\ln c_e}(\cdot)$	[-]	0.5	1.5	1	0.573	9.971e-04
k^-	[(A m⁻²)(m³ mol⁻¹)$^{(1+\alpha)}$]	7.5e-05	7.5e-03	7.5e-04	7.5e-05	4.457e-07
k^+	[(A m⁻²)(m³ mol⁻¹)$^{(1+\alpha)}$]	2.3e-04	2.3e-02	2.3e-03	2.3e-04	4.614e-06
R_f^-	[Ω m²]	1.0e-05	1.0e-03	5.0e-04	8.719e-05	6.773e-06
R_f^+	[Ω m²]	1.0e-04	1.0e-03	1.0e-03	4.619e-04	6.963e-06
$n_{Li,s}$	[mol]	-	-	-	0.1406	-
$c_e(x, 0)$	[mol m⁻³]	500	1500	1000	1500	8.191e-01

[†]Confidence interval calculated at the end of identification process in Figure 7d.

optimized input for that parameter. Note that parameter bounds are obtained from the literature[38–41] to ensure that the identified values are physically meaningful. Nominal parameter values that are away from the true parameter values could yield inaccurate sensitivities. To over-

Figure 8. Parameter estimates and 95% confidence intervals versus the nominal parameter values.

come this issue, we identify the most highly sensitive parameters at first to mitigate the negative effects as we accumulate the parameters to estimate. Furthermore, orthogonalized sensitivity analysis assists to determine the most significant parameters to model output. The results indicate that strongly identifiable parameters (e.g. $R_s^\pm$) have narrow confidence intervals while weakly identifiable parameters (e.g. $\sigma^\pm$) have relatively wide confidence intervals. This finding is intuitive, since large variations in the weakly identifiable parameters produce trivial changes in the voltage output trajectory, as demonstrated in Figure 5.

Validation

In this section, the proposed optimal experimental design (OED) is tested on various input profiles not used for identification, including driving cycles, sinusoidal inputs, and pulse inputs. In order to investigate the performance of the proposed approach, a "conventional" experimental design approach is considered for comparison. It consists of 7 standard constant charge/discharge profiles, along with a driving cycle. Unlike the proposed approach, the conventional approach does not group parameters, nor design inputs to maximize identifiability. All parameters of interest are identified from concatenating experimental data. The Levenberg-Marquardt algorithm is also utilized to fit parameter values. The parameters are fit using an "all-in-one" approach, meaning they are not grouped nor fit sequentially. All parameters are fit simultaneously.

Figures 9a and 9b compare the proposed and conventional approach to experimental constant discharge data with respect to battery capacity. These figures demonstrate that our proposed approach outperforms the conventional approach in terms of voltage accuracy. Table XII provides the RMSE on up to 90% of capacity range for the 0.5C and 1C discharge cases. Both experimental design approaches improve the model accuracy compared to nominal parameters. However, our proposed approach outperforms the conventional approach. Since we do not consider thermal parameters in this paper, the voltage prediction accuracy decreases as temperature evolves away from 25°C. Specifically, constant discharge at 1C is enough to produce non-trivial heat generation and cause surface temperature to nearly reach 30°C. The voltage prediction in the extremely low SOC region, such as below 3V, is difficult to match with experimental data. In this
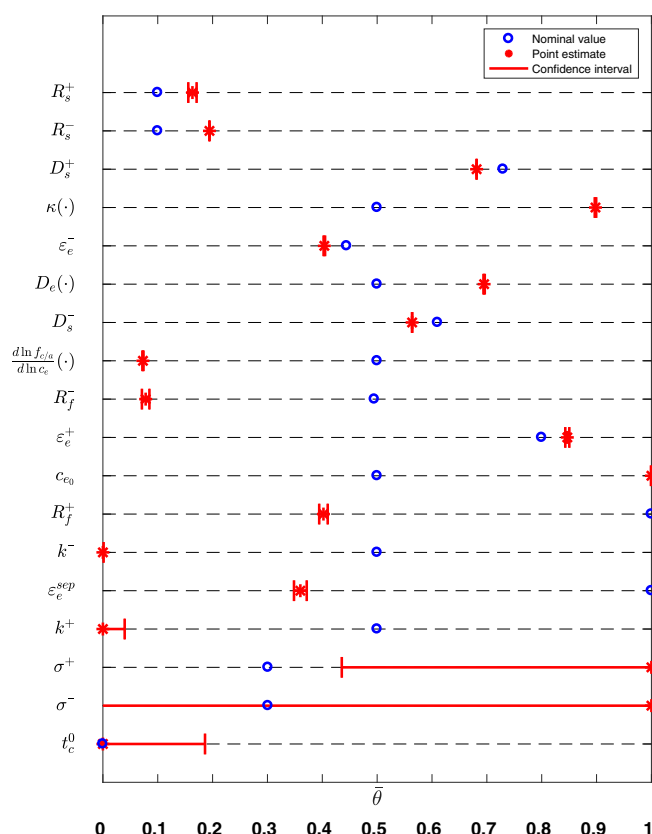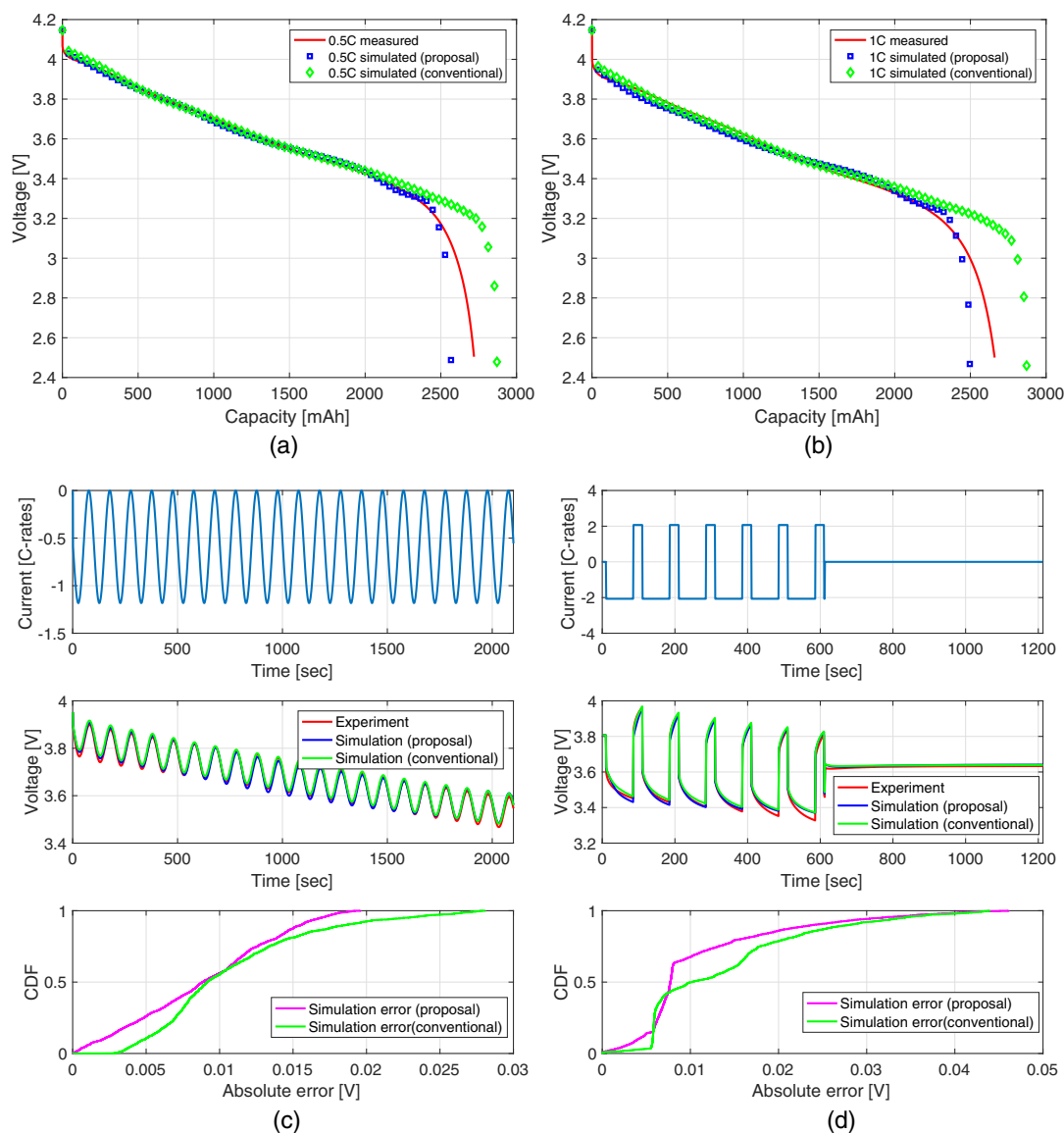
Figure 9. Experimental validation results for the NCA 18650 battery with testing profiles. (a) 0.5C validation with respect to discharge capacity. (b) 1C validation with respect to discharge capacity. (c) Sinusoidal input validation. (d) Pulse input validation.

region voltage drops dramatically and we have insufficient data sampling granularity to accurately identify the equilibrium structure. On the other hand, battery cells rarely operate in this region in practice.

Besides constant discharge tests, validation is also conducted on sinusoidal and pulse inputs to assure that the OED approach is able to capture a comprehensive set of input profiles. Figures 9c and 9d show the applied current profile and output voltage for sample sinusoidal and pulse inputs profiles. The voltage accuracy is calculated and summarized in Table XIII. Again, the OED approach outperforms the conventional approach.

Lastly, we use the driving cycle inputs described in TableVIII for validation. These driving cycles originate from automotive fuel emis-

sion testing. The RMSE calculations are summarized in Table XIV. The results show that the OED approach outperforms the conventional approach in every case.

Table XIII. RMSE between simulation and experimental measurement with sinusoidal and pulse inputs.

Input profiles	Errors in OED [mV]	Errors in conventional [mV]
Sinusoidal input	10.13	12.01
Pulse input	14.06	16.63

Table XIV. RMSE between simulations and experimental measurements with driving cycle inputs.

Input profiles	Errors in OED [mV]	Errors in conventional [mV]
DC 1	6.89	7.96
DC 2	8.49	12.50
LA 92	11.90	13.70
SC 04	14.50	17.20
UDDS	12.40	14.70

Table XII. RMSE between simulation and experimental measurement up to 90% capacity in constant discharge.

Parameters	0.5C discharge	1C discharge
Nominal parameters	33.7 mV	55.7 mV
Conventional approach	19.9 mV	36.1 mV
Proposed approach	11.8 mV	25.5 mV

Conclusions

In this work we have established an optimal experimental design (OED) framework for systematically identifying the parameters of an electrochemical battery model. We summarize our unique key contributions as follows.

1. A sensitivity analysis for the full-order electrochemical model, known as the Doyle-Fuller-Newman (DFN) model, is executed by deriving the sensitivity differential algebraic equations using Jacobians obtained via automatic differentiation. To the best of the authors' knowledge, an sensitivity analysis for all the electrochemical parameters has never been executed before. We place emphasis on this sensitivity analysis, as it plays a crucial role in computing the Fisher information matrix, and the parameter estimation algorithm via automatic differentiation.
2. We formulate an optimal experimental design via convex optimization. Rather than solving a large-scale nonlinear optimal control problem, we propose an input selection problem where the optimal inputs are selected from a (large) discrete set. Notably, we quantify the experimental output measurement variance for our battery tester to trade off Fisher information with measurement variance.
3. We provide the confidence intervals along with the parameter estimates via nonlinear least squares with the Levenberg-Marquardt algorithm.

We experimentally validate the performance of the proposed OED approach compared to conventional approach on a 18650 lithium nickel-cobalt-aluminum oxide (NCA) cell. We quantify the performance in terms of voltage accuracy with respect to experimentally measured voltage. We use a set of 9 validation profiles ranging from constant current pulses to driving cycles. The proposed approach achieves less than 15 mV RMSE in all validation scenarios, and outperforms the conventional approach in terms of voltage accuracy in all cases. Future work might involve further validation of the proposed OED framework using "synthetic" voltage and current data produced from a model with known parameter values.

Acknowledgments

Appendix A. Electrochemical Model

Solid phase diffusion of Li-ions.—The concentration of Li-ions in solid phase in the anode and cathode is govened by Fick's law.

$$\frac{\partial c_s^{\pm}}{\partial t}(x, r, t) = \frac{1}{r^2}\frac{\partial}{\partial r}\left[D_s^{\pm} r^2 \frac{\partial c_s^{\pm}}{\partial r}(x, r, t)\right]. \quad [A1]$$

The boundary conditions for the solid-phase diffusion PDE (A1) are

$$\frac{\partial c_s^{\pm}}{\partial r}(x, 0, t) = 0, \qquad \frac{\partial c_s^{\pm}}{\partial r}(x, R_s^{\pm}, t) = -\frac{1}{D_s^{\pm}} j_n^{\pm}. \quad [A2]$$

Eletrolyte diffusion of Li-ions.—The lithium concentration in the electrolyte changes due to concentration gradient-induced diffusive flow of ions and the current i_e.

$$\varepsilon_e^j \frac{\partial c_e^j}{\partial t}(x, t) = \frac{\partial}{\partial x}\left[D_e^{\text{eff}}(c_e^j)\frac{\partial c_e^j}{\partial x}(x, t) + \frac{1 - t_c^0}{F} i_e^j(x, t)\right], j \in \{-, sep, +\}. \quad [A3]$$

The boundary conditions for the electrolyte-phase diffusion PDE (A3) are given by

$$\frac{\partial c_e}{\partial x}(0^-, t) = \frac{\partial c_e}{\partial x}(0^+, t) = 0, \quad [A4]$$

$$D_e^{\text{eff},-}(c_e(L^-))\frac{\partial c_e}{\partial x}(L^-, t) = D_e^{\text{eff,sep}}(c_e(0^{\text{sep}}))\frac{\partial c_e}{\partial x}(0^{\text{sep}}, t), \quad [A5]$$

$$D_e^{\text{eff,sep}}(c_e(L^{\text{sep}}))\frac{\partial c_e}{\partial x}(L^{\text{sep}}, t) = D_e^{\text{eff},+}(c_e(L^+))\frac{\partial c_e}{\partial x}(L^+, t), \quad [A6]$$

$$c_e(L^-, t) = c_e(0^{\text{sep}}, t), \quad [A7]$$

$$c_e(L^{\text{sep}}, t) = c_e(0^+, t). \quad [A8]$$

Solid phase Ohm's law.—The solid potential is calculated from Ohm's law

$$\sigma^{\text{eff},\pm} \cdot \frac{\partial \phi_s^{\pm}}{\partial x}(x, t) = i_e^{\pm}(x, t) - I(t). \quad [A9]$$

The boundary conditions for the solid-phase potential ODE (A9) are given by

$$\frac{\partial \phi_s^-}{\partial x}(L^-, t) = \frac{\partial \phi_s^+}{\partial x}(L^+, t) = 0. \quad [A10]$$

Electrolyte Ohm's law.—The electrolyte potential is described by

$$\kappa^{\text{eff}}(c_e) \cdot \frac{\partial \phi_e}{\partial x}(x, t) = -i_e^{\pm}(x, t)$$
$$+\kappa^{\text{eff}}(c_e) \cdot \frac{2RT_1}{F}(1 - t_c^0) \cdot \left(1 + \frac{d\ln f_{c/a}}{d\ln c_e}(x, t)\right)\frac{\partial \ln c_e}{\partial x}(x, t). \quad [A11]$$

The boundary conditions for the electrolyte-phase potential ODE (A11) are given by

$$\phi_e(0^-, t) = 0, \quad [A12]$$

$$\phi_e(L^-, t) = \phi_e(0^{\text{sep}}, t), \quad [A13]$$

$$\phi_e(L^{\text{sep}}, t) = \phi_e(L^+, t). \quad [A14]$$

Electrolyte phase charge balance.—At each point in the electrode, the molar flux is related to the current in the electrolyte.

$$\frac{\partial i_e^{\pm}}{\partial x}(x, t) = a_s^{\pm} F j_n^{\pm}(x, t). \quad [A15]$$

The boundary conditions for the ionic current ODE (A15) are given by

$$i_e^-(0^-, t) = i_e^+(0^+, t) = 0. \quad [A16]$$

Butler-volmer kinetics.—The molar flux j_n depends on the concentration c_s of lithium in the solid, the concentration c_e of lithium in the electrolyte, and the solid-phase intercalation overpotential η is desribed by the Butler-Volermer equation.

$$j_n^{\pm}(x, t) = \frac{1}{F} i_0^{\pm}(x, t)\left[e^{\frac{\alpha_a F}{RT_1}\eta^{\pm}(x,t)} - e^{-\frac{\alpha_c F}{RT_1}\eta^{\pm}(x,t)}\right], \quad [A17]$$

where α_a and α_c are transport coefficients. The exchange current density i_0 is given by

$$i_0^{\pm}(x, t) = k^{\pm}\left[c_{ss}^{\pm}(x, t)\right]^{\alpha_c}\left[c_e(x, t)\left(c_{s,\max}^{\pm} - c_{ss}^{\pm}(x, t)\right)\right]^{\alpha_a}. \quad [A18]$$

The overpotential η corresponds to the reaction of solid-phase intercalation of lithium in the electrode.

$$\eta^{\pm}(x, t) = \phi_s^{\pm}(x, t) - \phi_e(x, t) - U^{\pm}(c_{ss}^{\pm}(x, t)) - FR_f^{\pm} j_n^{\pm}(x, t), \quad [A19]$$

$$c_{ss}^{\pm}(x, t) = c_s^{\pm}(x, R_s^{\pm}, t). \quad [A20]$$

The input to the model is the applied current density $I(t)$ [A m^{-2}], and the output is the voltage measured across the current collectors

$$V(t) = \phi_s^+(0^+, t) - \phi_s^-(0^-, t) - R_c I(t). \quad [A21]$$

Appendix B. Thermal Model

Two-state thermal model.—A two-state model is used to capture the lumped thermal dynamics of a cyliderical battery. This heat exchange is governed by convection and radiation between the battery core and ambient.

$$C_1 \frac{dT_1}{dt}(t) = h_{12}[T_2(t) - T_1(t)] + \dot{Q}(t), \quad [B1]$$

$$C_2 \frac{dT_2}{dt}(t) = h_{12}[T_1(t) - T_2(t)] + h_{2a}[T_{\text{amb}}(t) - T_2(t)], \quad [B2]$$

$$\dot{Q}(t) = I(t)\left[V(t) - [U^+(\bar{c}_s^+) - U^-(\bar{c}_s^-)] + T_1(t)\left[\frac{\partial U^+}{\partial T_1}(\bar{c}_s^+) - \frac{\partial U^-}{\partial T_1}(\bar{c}_s^-)\right]\right], \quad [B3]$$

where the bulk state of charge, $\bar{c}_s$ is given by

$$\bar{c}_s^{\pm}(x, t) = \frac{3}{(R_s^{\pm})^3} \int_0^{R_s^{\pm}} r^2 c_s^{\pm}(x, r, t) dr. \qquad [B4]$$

Temperature dependent parameters.—The parameters $D_s^{\pm}$, D_e, κ, $k^{\pm}$ vary with temperature via the Arrhenius relationship:

$$\psi = \psi_{\text{ref}} \exp\left[\frac{E_\psi}{R} \left(\frac{1}{T_1} - \frac{1}{T_{\text{ref}}} \right) \right], \qquad [B5]$$

where ψ represents a temperature dependent parameter, E_ψ is the activation energy [J mol^{-1}], and ψ_{ref} is the reference parameter value at reference temperature T_{ref}.

List of Symbols

Symbol	Description [SI units]
a_s	Specific interfacial surface area [m^2 m^{-3}]
A	Electrode Area [m^2]
c_s	Lithium concentration in solid phase [mol m^{-3}]
c_{ss}	Lithium concentration at surface in solid phase [mol m^{-3}]
c_e	Lithium concentration in electrolyte phase [mol m^{-3}]
$\frac{d \ln f_{c/a}}{d \ln c_e}$	Activity coefficient [-]
D_s	Diffusion coefficient in solid phase [m^2 s^{-1}]
D_e	Diffusion coefficient in electrolyte phase [m^2 s^{-1}]
F	Faraday constant [96487 coulomb mol^{-1}]
i	Ionic current [A m^{-2}]
I	Applied current density [A m^{-2}]
j	Molar ion flux [mol (m^2 s)$^{-1}$]
k	Kinetic rate constants [(A m^{-2})(m^3 mol^{-1})$^{(1+\alpha)}$]
$\dot{Q}$	Heat generation [W (m^{-2})]
$Q^{\pm}$	Electrode capacity [Ah]
Q	Voltage output variance [V^2]
R	Universal gas constant [8.3145 J (mol K)$^{-1}$]
R_c	Resistance of connectors [Ω m^2]
R_s	Radius of solid particles [m]
R_f	Solid-electrolyte inter-phase film resistance [Ω m^2]
t	Time [seconds]
t_c^0	Transference number [-]
T_1	Temperature at core[K]
T_2	Temperature at surface [K]
T_{amb}	Ambient temperature [K]
u	Input magnitude [-]
U	Open circuit potential of solid material [V]
V	Terminal voltage [V]
α	Charge transfer coefficients [-]
ε_s	Volume fraction in solid phase [-]
ε_e	Volume fraction in electrolyte phase [-]
η	Overpotential of an electrode [V]
θ^-	Negative electrode stoichiometry [-]
θ^+	Positive electrode stoichiometry [-]
κ	Electrolyte conductivity [S m^{-1}]
σ	Solid phase conductivity [S m^{-1}]
ϕ	Electric potential [V]
x	State variable vector [-]
y	Output vector [-]
z	Algebraic variable vector [-]
S	Sensitivity vector w.r.t parameters [-]
θ	Parameter vector [-]

ORCID

Saehong Park ⓘ https://orcid.org/0000-0002-0547-6345

References

1. N. A. Chaturvedi, R. Klein, J. Christensen, J. Ahmed, and A. Kojic, "Algorithms for Advanced Battery-Management Systems," *IEEE Control Systems*, **30**, 49 (2010).

2. and R. Klein, N. A. Chaturvedi, J. Christensen, J. Ahmed, R. Findeisen, and A. Kojic, "Electrochemical model based observer design for a lithium-ion battery," *IEEE Transactions on Control Systems Technology*, **21**, 289 (2013).

3. A. P. Schmidt, M. Bitzer, A.W. Imre, and L. Guzzella, "Experiment-driven electrochemical modeling and systematic parameterization for a lithium-ion battery cell," *Journal of Power Sources*, **195**, 5071 (2010).

4. A. M. Bizeray, J. Kim, S. R. Duncan, and D. A. Howey, "Identifiability and parameter estimation of the single particle lithium-ion battery model,"*Submitted to IEEE Transactions on Control Systems Technology*,

5. J. C. Forman, S. J. Moura, J. L. Stein, and H. K. Fathy, "Genetic identification and fisher identifiability analysis of the Doyle-Fuller-Newman model from experimental cycling of a LiFePO 4 cell," *Journal of Power Sources*, **210**, 263 (2012).

6. L. Zhang, L. Wang, G. Hinds, C. Lyu, J. Zheng, and J. Li, "Multi-objective optimization of lithium-ion battery model using genetic algorithm approach," *Journal of Power Sources*, **270**, 367 (2014).

7. L. Zhang, C. Lyu, G. Hinds, L. Wang, W. Luo, J. Zheng, and K. Ma, "Parameter sensitivity analysis of cylindrical LiFePo$_4$ battery performance using multi-physics modeling ," *Journal of Electrochemical Society*, **161**, A762 (2014).

8. R. Jobman, "Identification of Lithium-Ion Physics-Based Model Parameter Values," *Ph.D. Thesis*, University of Colorado, Colorado Springs, 2016.

9. N. Jin, D. L. Danilov, P. M. J. Van den Hof, and M. C. F. Donkers, "Parameter estimation of an electrochemistry-based Lithium-ion battery model using a two-step procedure and a parameter sensitivity analysis," *Draft*.

10. J. Marcicki, M. Canova, A. T. Conlist, and G. Rizzoni, "Design and parametrization analysis of a reduced-order electrochemical model of graphite/LiFePO$_4$ cells for SOC/SOH estimation," *Journal of Power Sources*, **237**, 310 (2013).

11. J. Vazquez-Arenas, L. E. Gimenez, M. Fowler, T. Han, and S. K. Chen, "A rapid estimation and sensitivity analysis of parameters describing the behavior of commercial Li-ion batteries including thermal analysis," *Energy Conversion and Management*, **87**, 472 (2014).

12. M. J. Rothenberger, J. Anstrom, S. Brennan, and H. K. Fathy, "Maximizing Parameter Identifiability of an Equivalent-Circuit Battery Model Using Optimal Periodic Input Shaping," *2014 ASME Dynamic Systems and Control Conference*, 2014.

13. J. Liu, M. Rothenberger, S. Mendoza, P. Mishra, Y. Jung, and H. K. Fathy, "Can an Identifiability-Optimizing Test Protocol Improve the Robustness of Subsequent Health-Conscious Lithium-ion Battery Control? An Illustrative Case Study," *2016 American Control Conference*, 2016.

14. G. Franceschini and S. Macchietto, "Model-based design of experiments for parameter precision: State of the art," *Chemical Engineering Science*, **63**, 4846 (2008).

15. K. E. Thomas, J. Newman, and R. M. Darling, "Mathematical modeling of lithium batteries," *Advances in lithium-ion batteries*, Springer, pp. 345-392, 2002.

16. X. Lin, H. E. Perez, S. Mohan, J. B. Siegal, A. G. Stefanopoulou, Y. Ding, and M. P. Castanier, " A lumped-parameter electro-thermal model for cylindrical batteries," *Journal of Power Sources*, **257**, 1 (2014).

17. V. R. Subramanian, V. Boovaragavan, V. Ramadesigan, and M. Arabandi, "Mathematical model reformulation for lithium-ion battery simulations: Galvanostatic boundary conditions," *Journal of Electrochemical Society*, **156**, A260 (2009).

18. J. C. Forman, S. Bashash, J. L. Stein, and H. K. Fathy, "Reduction of an electrochemistry-based li-ion battery model via quasi-linearization and pade approximation," *Journal of Electrochemical Society*, **158**, A93 (2011).

19. G. Fan, K. Pan, and M. Canova, "A comparison of model order reduction techniques for electrochemical characterization of lithium-ion batteries, " in *2015 IEEE Decision and Control Conference*, 3922, 2015.

20. A. M. Bizeray, S. Zhao, S. R. Duncan, and D. A. Howey, " Lithium-ion battery thermal-electrochemical model-based state estimation using orthogonal collocation and a modified extended Kalman filter," *Journal of Power Sources*, **296**, 400 (2015).

21. H. Yue, M. Brown, F. He, J. Jia, and D. B. Kell, " Sensitivity analysis and robust experimental design of a signal transduction pathway system," *International Journal of Chemical Kinetics*, **40**, 730 (2008).

22. H. Khalil, " Nonlinear systems ", Prentice Hall, 2002.

23. A. Joel, "A General-Purpose Software Framework for Dynamic Optimization,"*Ph.D. Thesis*, Areberg Doctorl School, KU Leuven, 2013.

24. A. C. Hindmarsh, P. N. Brown, K. E. Grant, S. L. Lee, R. Serban, D. E. Shumaker, and C. S. Woodward, "SUNDIALS: Suite of nonlinear and differential/algebraic equation solvers," *ACM Transactions on Mathematical Software (TOMS)*, **31**, 363 (2005).

25. N. Chaturvedi, R. Klein, J. Christensen, J. Ahmed, and A. Kojic, " Method and system for estimating a capacity of individual electrodes and the total capacity of a lithium-ion battery system, "*Patents*, EP 20,140,707,912, 2016.

26. D. LeBlanc, " Road departure crash warning system field operational test: methodology and results. volume 1: technical report, "*Technical Report.*, University of Michigan, Ann Arbor, 2006.

27. Environmental protection agency, " Vehicle and Fuel Emission Testing, "*Technical Report*.

28. B. F. Lund and B. A Foss, " Parameter ranking by orthogonalization-applied to nonlinear mechanistic models," *Automatica*, **44**, 278 (2008).

29. A. Bjorck, " Solving linear least squares problems by Gram-Schmidt orthogonalization," *BIT Numerical Mathematics*, **7**, 1 (1967).

30. E. Walter and L. Pronzate, "Identification of parametric models from experimental data,"*Springer Verlag*, 1997.

31. T. M. Cover and J. A. Thomas, " Elements of information theory,"*John Wiley & Sons*, 2012.

32. K. Chaloner and I. Verdinelli, "Statistical Science,"*JSTOR*, 273, (1995).
33. M. Grant and S. Boyd, "CVX: Matlab Software for Disciplined Convex Programming, version 2.1 ", 2014.
34. S. Boyd, "Convex optimization", Cambridge university press, 2009.
35. K. Levenberg, " A method for the solution of certain non-linear problems in least squares," *Quarterly of applied mathematics*, **2**, 164 (1944).
36. W. N. Venables and B. D. Ripley, "Modern applied statistics with S-PLUS, "Springer Science & Business Media, (2013).
37. S. Park, K. Kato, Z. Gima, R. Klein, and S. Moura, accepted in "Optimal Input Design for Parameter Identification in an Electrochemical Li-ion Battery Model, "*2018 American Control Conference*, 2018.
38. W. Fang, O. Kwon, and C. Wang, "Electrochemical–thermal modeling of automotive Li-ion batteries and experimental validation using a three-electrode cell,"*International journal of energy research*, 2010.
39. D. M. Bernardi and J. Go, " Analysis of pulse and relaxation behavior in lithium-ion batteries," *Journal of Power Sources*, **196**, 412 (2011).
40. K. Uddin, S. Perera, W. D. Widanage, L. Somerville, and J. Marco, " Characterising lithium-ion battery degradation through the identification and tracking of electrochemical battery model parameters," *Batteries*, **2**, 13 (2016).
41. T. R. Ashwin, A. McGordon, D. Widanage, and P. A. Jennings, "Modified electrochemical parameter estimation of NCR18650BD battery using implicit finite volume method," *Journal of Power Sources*, **341**, 387 (2017).